RSC Pharmaceutics

ROYAL SOCIETY OF CHEMISTRY

PAPER

View Article Online
View Journal | View Issue

Cite this: *RSC Pharm.*, 2025, **2**, 541

Artesunate-loaded bilosomes with enhanced oral bioavailability: *in silico* and *in vitro* study against *Leishmania donovani* promastigotes and *in vivo* pharmacokinetic assessment in rats

Hitesh Wankhede,[a] Sudha Madhavi Penumaka,[b] Debabrata Mandal,[b] Supada Rojatkar,[c] Vinod Gaikwad[d] and Sharvil Patil *[a]

The deadly parasite disease known as visceral leishmaniasis (VL) is caused by the protozoa of *Leishmania donovani*. Artesunate (ART) has been reported to act against VL. However, its medical use is limited owing to the fact that it belongs to BCS class II. Thus, the aim of the present work was to prepare ART-loaded bilosomes (ART-BIL) to mitigate the drawbacks associated with ART. Box–Behnken design was used to optimize ART-BIL prepared by the ethanol injection method. ART-BIL were characterized for vesicle size, entrapment efficiency, FTIR, DSC, TEM, *in vitro* drug release, *in silico* molecular docking, *in vitro* antileishmanial activity against *Leishmania donovani*, and *in vivo* pharmacokinetic assessment. The optimized spherical ART-BIL was found to have a vesicle size of 186.7 ± 15.0 nm and an entrapment efficiency of 95.36 ± 2.5%. Spherical, non-aggregated vesicles demonstrated a biphasic drug release profile with a remarkable increase in the dissolution rate of artesunate compared to an artesunate dispersion. *In silico* molecular docking studies revealed the antileishmanial potential of artesunate and chenodeoxycholic acid by binding them to glyceraldehyde 3-phosphate dehydrogenase (G3PDH). Further, *in vitro* antileishmanial studies showed a significant enhancement in the antileishmanial potential of artesunate while *in vivo* pharmacokinetic studies demonstrated 1.39 and 1.47 fold increases in the C_{max} and AUC of ART when formulated into bilosomes. ART-loaded bilosomes could be a promising drug delivery system for the treatment of visceral leishmaniasis.

Received 25th January 2025,
Accepted 1st March 2025

DOI: 10.1039/d5pm00025d

rsc.li/RSCPharma

1. Introduction

Leishmaniasis is becoming a more serious public health issue. A group of parasitic diseases referred to as leishmaniasis are caused by an intracellular parasite transmitted by the bite of a *Lutzomyia* parasite or an infected female *Phlebotomus* sand fly. Clinical manifestations of leishmaniasis range from minor skin lesions to severe mucosal/cutaneous symptoms and a fatal visceral form in some cases. Leishmaniasis is reported to occur in more than 100 countries, spanning from warm temperate through subtropical to tropical climates.[1] *Leishmania donovani* complex protozoa (*L. donovani* and *L. infantum*) are the culprits behind visceral leishmaniasis (VL), frequently referred to as kala-azar, a crippling disease which impacts more than 200 million individuals in 62 countries and is estimated to cause 500 000 new cases and 60 000 deaths annually.[2] There are two types of the parasite: amastigote and promastigote. Amastigotes (both axenic and intracellular) continue to proliferate slowly, have a diminished ability for biosynthesis, a lower amount of bioenergy, and a markedly altered metabolism. A female sand fly takes the parasites and a blood meal from an affected individual, wherein the parasites develop into virulent (metacyclic) promastigote forms after changing from amastigotes to procyclic promastigotes.[3] The parasite's promastigote form infects mammals as hosts. VL causes serious health issues as well as fatalities. Over 90% of instances are found in Brazil, Bangladesh, India, Nepal, and Sudan. Leishmaniasis can be in cutaneous, mucocutaneous, or visceral form. A chronic protozoan infection, *i.e.* VL, is brought on by a parasite of the genus *Leishmania*.[4] The parasite survives and reproduces within the reticuloendothelial system of

[a]*Bharati Vidyapeeth (Deemed to be University), Poona College of Pharmacy, Department of Pharmaceutics, Erandwane, Pune, 411 038 Maharashtra, India. E-mail: sharvilpatil25@gmail.com, sharvil.patil@bharatividyapeeth.edu; Fax: +91 20 25439383; Tel: +91 20 25437237*
[b]*Department of Biotechnology, National Institute of Pharmaceutical Education and Research (NIPER) Hajipur (844 102), Bihar, India*
[c]*Research & Development Centre in Pharmaceutical sciences and Applied Chemistry, Bharati Vidyapeeth (Deemed to be University), Poona College of Pharmacy Campus, Erandwane, Pune 411038, Maharashtra, India*
[d]*Department of Pharmaceutics, National Institute of Pharmaceutical Education and Research (NIPER) Hajipur (844 102), Bihar, India*

macrophages. If treatment is not received, VL is linked to significant immunological dysfunction and high mortality.[5] The parasite causes hepatosplenomegaly, anaemia, hypergammaglobulinemia, and persistent immunosuppression by infecting reticuloendothelial system cells. The successful treatment of VL shows restoration of Th1-biased response and suppression of the Th2 cytokines that facilitate parasite elimination.[6] One of the critical routes for the survival of the *Leishmania* parasite in a human host is the glycolytic pathway. The parasite obtains energy in the form of adenosine triphosphate (ATP) through the glycolytic pathway.[7–9] Therefore, it may be considered a great idea to use different compounds to block the glycolytic pathways which act as a source of energy for the parasite in the host body. Numerous enzymes that are part of the leishmania glycolytic pathway are crucial to the cascade of the glycolysis system, like glyceraldehyde-3-phosphate isomerase,[10,11] glyceraldehyde-3-phosphate dehydrogenase,[12] pyruvate kinase,[13] and triosephosphate isomerase.[14] As vaccinations are currently unavailable, chemotherapy is the sole available treatment for VL.

Amphotericin B and pentavalent antimonials are part of the current regimen treating VL, such as liposomal amphotericin B, miltefosine, and paromomycin, all of which are inadequate due to their high cost, toxicity, and occasional resistance.[15] Considering the aforementioned limitations, drugs such as artemisinin and artesunate (ART) derived from *Artemisia annua* have been used to treat a variety of parasitic and protozoan illnesses. In addition to anti-malarial activity, ART has demonstrated potential in a wide range of forms of cancer, including hepatocarcinoma, colorectal cancer, breast cancer, and lung cancer.[16–19] There are reports that indicate that a higher safety index and antileishmanial activity can be achieved both *in vitro* and *in vivo* with very few negative effects for ART in the host body.[20,21] However, despite its therapeutic benefits, ART has significant drawbacks, such as low aqueous solubility and instability in the intestines that result in poor oral bioavailability, limiting its clinical utility.[22]

A nano-medication delivery method is a sensible option to improve the water solubility and therapeutic impact of ART. Most drug delivery systems rely heavily on lipid-based vesicular systems owing to their advantages, such as the ability to encapsulate both hydrophilic and lipophilic medication, high drug loading and resolving the insolubility issue of drug molecules by using nanosize molecules.[23] Bilosomes (BIL) are superior drug delivery systems compared to other lipid-based vesicular systems, as they are more elastic, flexible, and ultra-deformable, with an ability to shield drugs from enzymatic degradation in the gastrointestinal tract.[24] In the case of conventional vesicles such as liposomes and niosomes, the presence of intestinal bile salt in the GIT restricts their effectiveness, as it causes vesicle membrane deformation and lysis, ultimately releasing the encapsulated molecule prematurely before it reaches the target site of action.[25] However, BIL are bile-salt-stabilized nanovesicular systems consisting of bile salts incorporated into lipid bilayers. BIL are more stable as they are well organized, which causes them repulsion to the intestinal bile salts in the GIT.[26] Additionally, the bile salts are known to be natural intestinal permeation enhancers in the body that increase the oral bioavailability of medications with limited water solubility and intestinal permeability.[27] Moreover, BIL demonstrate the capacity to migrate through Peyer's patches (M cells) in the GIT, hence augmenting the oral bioavailability of most of the molecules. The gastrointestinal stability of these nano-vesicular carrier systems is enhanced by a variety of bile salts, such as sodium taurocholate (STC), sodium deoxycholate (SDC), and sodium glycocholate (SGC). Considering its safety and ability to enhance the permeation of molecules significantly, SDC is the most widely utilized of amongst them[28] Furthermore, chenodeoxycholic acid (CDCA), a novel component of bile salts, has demonstrated significant antileishmanial activity because of its immunomodulatory activity, limiting the parasite burden and infectivity *in vivo* in mouse models. This illustrates the ability of CDCA to both enhance the host's advantageous immune cytokine responses (Th1) and inhibit its undesirable immune activity (Th2 cytokine responses).[29]

Thus considering the benefits associated with BIL, it was thought that ART could be formulated into BIL, mitigating drawbacks associated with it. The ethanol injection method was used to prepare ART-loaded bilosomes (ART-BIL) and Box–Behnken design (BBD) was used for batch optimization. ART-BIL were characterized for vesicle size, entrapment efficiency, Fourier transform infrared spectroscopy (FTIR), differential scanning calorimetry (DSC), transmission electron microscopy (TEM), *in vitro* drug release, *in silico* molecular docking, *in vitro* antileishmanial activity against *Leishmania donovani*, and *in vivo* pharmacokinetic assessment.

2. Material and methods

2.1 Materials

ART, sodium deoxycholate (98% pure) was purchased from Alpha Chemika, Mumbai, Maharashtra. Chenodeoxycholic acid, Poloxamer 407, cholesterol, ethanol, acetonitrile, and methanol were procured from Loba Chemicals, Mumbai, India. A dialysis bag with a molecular weight cut-off of 12 000 kDa with 22.54 mm width was purchased from HIMEDIA Laboratory (Mumbai, India). Analytical-grade chemicals and reagents were used for the study.

2.2 Method

2.2.1 Preparation of ART-loaded bilosomes. A slightly modified version of the ethanol injection method was used to formulate ART-loaded bilosomes (ART-BIL). ART (25 mg), cholesterol, and chenodeoxycholic acid (3 mg) were dissolved in ethanol (2 mL, the organic phase). A surfactant (Poloxamer 407)/BS (SDC) solution (10 mL) was used as an aqueous phase. Both solutions (organic and aqueous) were heated to 40–50 °C. The organic phase was gradually added to the surfactant solution with constant stirring. The dispersion was continuously

Table 1 Formulation of batches of ART-BIL using Box–Behnken design

Run	Factor 1 A: Cholesterol (mg)	Factor 2 B: SDC (mg)	Factor 3 C: Poloxamer 407 (mg)	Response 1 Vesicle size, nm	Response 2 %EE
1	−1 (10)	0 (60)	−1 (30)	211 ± 7.83	89.1 ± 2.42
2	0 (12.5)	0 (60)	0 (60)	266 ± 4.46	91 ± 2.00
3	+1 (15)	0 (60)	+1 (90)	277 ± 5.53	94.51 ± 1.12
4	0 (12.5)	+1 (90)	−1 (30)	253 ± 4.3	91.3 ± 1.14
5	−1 (10)	−1 (30)	0 (60)	180 ± 3.16	92 ± 2.11
6	+1 (15)	+1 (90)	0 (60)	290.5 ± 1.60	94.58 ± 3.22
7	+1 (15)	0 (60)	−1 (30)	280 ± 5.56	96.9 ± 2.04
8	0 (12.5)	0 (60)	0 (60)	258.3 ± 2.44	92 ± 2.15
9	+1 (15)	−1 (30)	0 (60)	268 ± 3.25	96.89 ± 3.56
10	0 (12.5)	0 (60)	0 (60)	260.1 ± 4.59	92 ± 1.12
11	0 (12.5)	0 (60)	0 (60)	250.8 ± 3.59	92 ± 2.11
12	0 (12.5)	0 (60)	0 (60)	248.4 ± 2.79	92 ± 3.02
13	−1 (10)	0 (60)	+1 (90)	169 ± 3.84	92.41 ± 2.15
14	−1 (10)	+1 (90)	0 (60)	190 ± 4.20	89 ± 1.14
15	0 (12.5)	+1 (90)	+1 (90)	255.1 ± 3.08	92 ± 3.22
16	0 (12.5)	−1 (30)	+1 (90)	190 ± 1.92	95.45 ± 3.09
17	0 (12.5)	−1 (30)	−1 (30)	235 ± 4.06	93.3 ± 2.00

stirred for 6 hours at 50–55 °C until all of the ethanol had evaporated to obtain the bilosomes (Table 1).

Various independent and dependent variables (vesicle size and entrapment efficiency) were taken into account when developing ART-BIL formulations utilizing BBD (Table 1).

2.2.2 Optimization. BBD, which is one of the preferred designs as it gives more data in fewer runs (17 runs), was utilized for the formulation of ART-BIL. Design-Expert software (Design-Expert©; version 13; Stat-Ease Inc., Minneapolis, USA) was used to implement BBD as yield results by avoiding extreme star points and factorial points for the same number of factors, which eliminates the need to test extreme values of factors. The independent variables were cholesterol (A, CHO), BS (B, SDC), and surfactant (C, P407) at three different levels: low (−1), medium (0), and high (+1). The amount of ART (25 mg) and CDCA (3 mg) was kept constant for all batches. The responses were recorded in terms of vesicle size (Y1, VS) and percentage entrapment efficiency (Y2, %EE) (Table 1). The criteria for selecting the optimal formulation were kept as the minimum vesicle size and maximal %EE.

2.2.3 Preparation of aqueous dispersion of ART (ART-dispersion). ART alone (25 mg) was dispersed in 10 mL of distilled water using a Vibra-Cell™ VCX500 ultrasound probe sonicator (Sonics & Materials, Inc., USA).

2.3. Characterization

2.3.1 Vesicle size (VS). A Nano ZS zetasizer (HORIBA ZS-100) was used to estimate the vesicle size of the prepared batches. The instrument works on the principle of dynamic light scattering. Prior to measurement, 0.1 mL of ART-BIL was diluted 100 times using Millipore water. The samples were scanned with a 90° incidence angle, keeping a refractive index value of 1.33.

2.3.2 Percentage entrapment efficiency (%EE). The amount of ART entrapped in BIL was measured by the ultracentrifugation technique. An ART-BIL dispersion (2 mL) was put into an Allegra 64R centrifuge tube, and the tube was centrifuged for 30 min at 4 °C at 15 000 rpm. Before free ART was quantified, the obtained supernatant was decanted and suitably diluted with Millipore water.[30] A UV-visible spectrophotometer (Jasco, model V-730A PC, Kyoto, Japan) was used to measure the amounts of entrapped and unentrapped of ART. %EE was determined mathematically using eqn (1):

$$\mathrm{EE}\,(\%) = \frac{\text{Total drug} - \text{Free drug in supernatent}}{\text{Total drug}} \times 100 \quad (1)$$

2.3.2.1 Optimization of formulation. A point prediction algorithm was used to optimize the formulation. The criteria of minimum VS and maximum %EE were used to select the best formulation. The composite desirability value was also estimated to assess the robustness of the optimized formulation. The prediction error was also estimated using eqn (2) to confirm the validity of the obtained responses:

$$\text{Prediction error} = \frac{\text{predicted value} - \text{observed value}}{\text{observed value}} \times 100 \quad (2)$$

2.3.3 Evaluation of artesunate-excipient compatibility using FTIR. An FTIR spectrophotometer FTIR-8400 (JASCO, Tokyo, Japan) was used to record the FTIR spectra of ART alone, CHO, P407, SDC, CDCA, and a lyophilized optimized ART-BIL dispersion (ART-BILopt) in the 400–4000 cm^{-1} range. A sample (approx. 10 mg) was triturated in a mortar with KBr (50 mg). To record the spectra, the powder was placed inside the IR slots. The distinctive bands in every sample were recorded using the FTIR 8000 SCS program (Prague, Czech Republic).

2.3.4 Thermal analysis of ART and excipient using DSC. A DSC 821e differential scanning calorimeter (Mettler-Toledo, Greifensee, Switzerland) was used to perform thermal analysis of ART alone, SDC, CHO, P407, CDCA, and lyophilized ART-BILopt. Samples (3–5 mg each) were placed into a conventional aluminium pan, which was then hermetically sealed.

The pan was heated under an inert nitrogen flow at a rate of 10 mL min^{-1}.

2.3.5 Examination of bilosome morphology using TEM. Transmission electron microscopy (TEM, Tecnai 12, operating potential 120 kV, ICON Labs, Navi Mumbai,) was used to reveal the surface morphology and vesicle size of ART-BILopt. The dispersion drops were poured onto the copper grid and allowed to air dry before measurement.

2.3.6 Estimation of *in vitro* ART release from ART-BIL. The drug release pattern of the ART dispersion and ART-BILopt was assessed using the dialysis bag technique. Before the study began, the dialysis bag (diameter 16 mm, molecular weight cut off: 12 000 g mol^{-1}) was pre-treated and activated by immersing it in the dissolution medium (aqueous phase) for a full day.[31] A pre-treated dialysis sac containing ART-BILopt corresponding to 5 mg of ART was sealed on both sides and submerged for 2 h in a freshly made acidic medium (pH 1.2) (50 mL). Then it was transferred to pH 6.8 for the final 24 h. The release medium (37 ± 0.5 °C) was rotated at 100 rpm, using a magnetic stirrer (REMI 1MLH). A predefined volume (1 mL) of sample was taken out and replaced with fresh release medium (same volume) at predefined time intervals of 0.5, 1, 2, 4, 6, 8, 10, 12, 24 h. An identical experimental setup was used for the ART dispersion release. Lastly, using a UV spectrophotometer set to 242 nm, the collected samples were analysed with appropriate dilutions.

2.3.7 Estimation of binding potential of ART and CDCA using an *in silico* docking study. PyMOL version 2.5.4 (The PyMOL Molecular Graphics System, Version 2.0 Schrödinger, LLC) and AutoDockTools-1.5.7 were used for optimization of ligand and protein. For ligand optimization, the geometry of the ligands was cleaned, whereas for protein, the water was removed. The docking was performed using AutoDockTools 1.5.7. The docking analyses were performed using both PyMOL and BIOVIA Discovery Studio 4.5 (BIOVIA, D.S 2019).

2.3.7.1 Selection of ligand. It has been reported that CDCA shows protective and immunomodulatory activity which is also beneficial in VL, and ART has strong antileishmanial activity against *Leishmania donovani*, which is a causative agent in VL.[32,33] We performed *in silico* molecular docking studies using ART and CDCA as ligands in order to determine the validity of the hypothesis regarding antileishmanial activity and to investigate any potential synergistic (immunomodulatory) or targeting ability of CDCA when used with ART.

2.3.7.2 Selection of protein. The literature reports that ART inhibits glycerol 3-phosphate dehydrogenase to demonstrate antileishmanial activity.[20] In addition to demonstrating therapeutic antileishmanial activity, we conducted molecular docking experiments with both ligands (ART and CDCA) and enzyme/protein (glycerol 3-phosphate dehydrogenase) to investigate potential interactions or positive effects of CDCA.

2.3.7.3 Preparation of ligands. The SDF file containing the 2D structures of ART and CDCA was obtained from PubChem. PyMOL software was used to transform the SDF file of ART and CDCA was transformed into a PDB file.

2.3.7.4 Preparation of receptors. The Protein Data Bank (PDB) provided the three-dimensional (3D) structures of the enzyme. All heteroatoms, such as water, except amino acids, were eliminated from the enzyme design in order to improve it.

2.3.7.5 Docking study. Molecular docking was performed using AutoDock Vina 1.1.2 and AutoDockTools 1.5.7. Ligands and proteins were converted to pdbqt format. AutoDock Vina split was used to divide the results. The literature was explored for active places for the grid box preparation. The architectural requirements dictated the dimensions of the grid box, and all other parameters were left at their default settings. The dimensions of the grid box were $x = 40$, $y = 40$, and $z = 40$. Following the docking process, the most stable conformation was selected for additional assessment. H-bond interactions were seen in Discovery Studio 2021.

2.4 *In vitro* evaluation of ART-BIL against leishmanial promastigotes

Leishmania donovani (MHOM/1983/AG83) cells (promastigotes) were routinely cultured in M199 media supplemented with 10% FBS and allowed to grow in an incubator at 24 °C. Log phase cells (1×10^6 mL^{-1}) were treated with ART, ART-BIL (A-B), blank BIL and CDCA with concentrations of 10 and 50 μg mL^{-1} for 3 days. The cell viability was measured by Trypan blue exclusion and the 3-(4,5-dimethylthiazol-2-yl)-2,5-diphenyltetrazolium bromide (MTT)-based reduction method every 24 h using known procedures. Amphoterin B (AmB)-treated (50 nM) and untreated parasites were used as positive and negative controls, respectively. Compared to untreated cells, the number of viable parasites, under each treatment condition, was calculated on a percentage scale and presented in bar graphs. After 48 h, the concentration of the drug/formulation showing 50% killing of the *L. donovani* promastigotes was considered IC_{50} for that drug or formulation.[34,35]

2.5 *In vivo* pharmacokinetic evaluation of ART-BIL

A study of the *in vivo* pharmacokinetics of ART-BILopt and ART dispersion was conducted on male Wistar rats weighing between 180 and 250 g. Before the trial began, the animals had unlimited access to food and water at a temperature of 25 °C and 50% relative humidity. Two sets of animals, each consisting of six rats, were used in the investigation. In India, the Institutional Animal Ethics Committee is managed and controlled by the Control and Supervision of Experiments on Animals (CPSEA) committee, which was established in accordance with The Prevention of Cruelty to Animal Act 1960. The Bharati Vidyapeeth Poona College of Pharmacy's institutional animal ethics committee authorized the study protocol, which was approved by CPSEA (Approval No. PCP/IAEC/2024/1-16). The National Institutes of Health's Handbook for the care and use of laboratory animals (NIH Publications No. 8023, amended 1978) and the ARRIVE criteria were followed in all animal experiments. Group 1 received ART dispersion administration, while Group 2 received ART-BILopt (equivalent to 150 mg kg^{-1} of ART) *via* an 18-gauge oral feeding needle.[35] The rats were anaesthetized using diethyl ether in order to

remove a blood sample (2 mL) from the retro-orbital plexus at time intervals of 0.5, 1, 2, 4, 6, 8, 10, 12, and 24 h in microcentrifuge tubes coated with EDTA. The plasma was then separated from the obtained samples by centrifuging them for 15 min at 4 °C at 10 000 rpm. ART contained in plasma was extracted using an acetone : methanol (1 : 1 v/v) mixture. Before being injected into an HPLC column, the supernatant was dried to dissolve it in acetonitrile. The quantity of ART in the extracted samples was estimated using RP-HPLC fitted with a binary pump and a UV detector. A mixture of water and acetonitrile (pH 3) in 90 : 10 (v/v) ratio was used as the mobile phase with a C-18 column as the stationary phase (Thermo Fisher Scientific 250 mm, 4.5 mm). The runtime was 10 minutes and the wavelength was set at 242 nm. For the 20 μL injected sample, the pump flow rate was 1 mL min^{-1}.[36] Using the one-compartment open model and the PKSolver Pk2 program, the area under the curve (AUC), maximum plasma concentration (C_{max}), time to achieve maximum plasma concentration (T_{max}), plasma half-life ($t_{1/2}$), and elimination rate constant (K_{el}) were estimated.

2.6 Statistical analysis

All the studies were conducted in triplicate. The results are presented as a mean with standard deviation. GraphPad Prism software was used to perform the statistical calculations. $P < 0.05$ was regarded as statistically significant.

3. Results

Trial batches were produced in the early research using ART, CHO, BS, and CDCA. Nevertheless, BIL aggregation was noted. Several steps were taken to stabilize the BIL dispersion. Research was conducted using TPGS, Span, Tween series, Poloxamer 188, and Poloxamer 407, in a range of ratios, concentrations, and cholesterol concentrations. Finally, based on vesicle size and stability, Poloxamer 407 was used as a stabilizer. Batch optimization was carried out using CHO, P407, SDC, and CDCA.

3.1 Experimental design optimization

Factorial designs, such as Box–Behnken design, are employed to concurrently look at how different variables affect a response. In the experimental runs, the effects of cholesterol (A), surfactant (B), and bile salt (C) were examined on vesicle size (Y1) and %EE (Y2) responses.

3.1.1 Impact of independent variables on vesicle size. ART-BIL was optimized using 3-factor, 3-level BBD (Table 1). The lowest and maximum vesicle diameters of ART-BIL were determined to be between 169 and 290.5 nm. A polynomial equation (eqn (3)) and Fig. 1A demonstrate the effect of the independent variables on vesicle size. The positive sign of a coefficient in a polynomial equation suggests a direct relationship, while a negative sign denotes an inverse relationship between the response and the independent variable.

$$\begin{aligned}\text{Vesicle size} = {} & +256.72 + 45.69 \times A \\ & + 14.45 \times B - 10.99 \times C + 3.12 \times AB + 9.75 \times AC \\ & + 11.78 \times BC - 11.81 \times A^2 - 12.79 \times B^2 - 10.66 \times C^2\end{aligned} \quad (3)$$

The adjusted (0.9457) and expected (0.7495) R^2 values showed good agreement. In order for an agreement to be

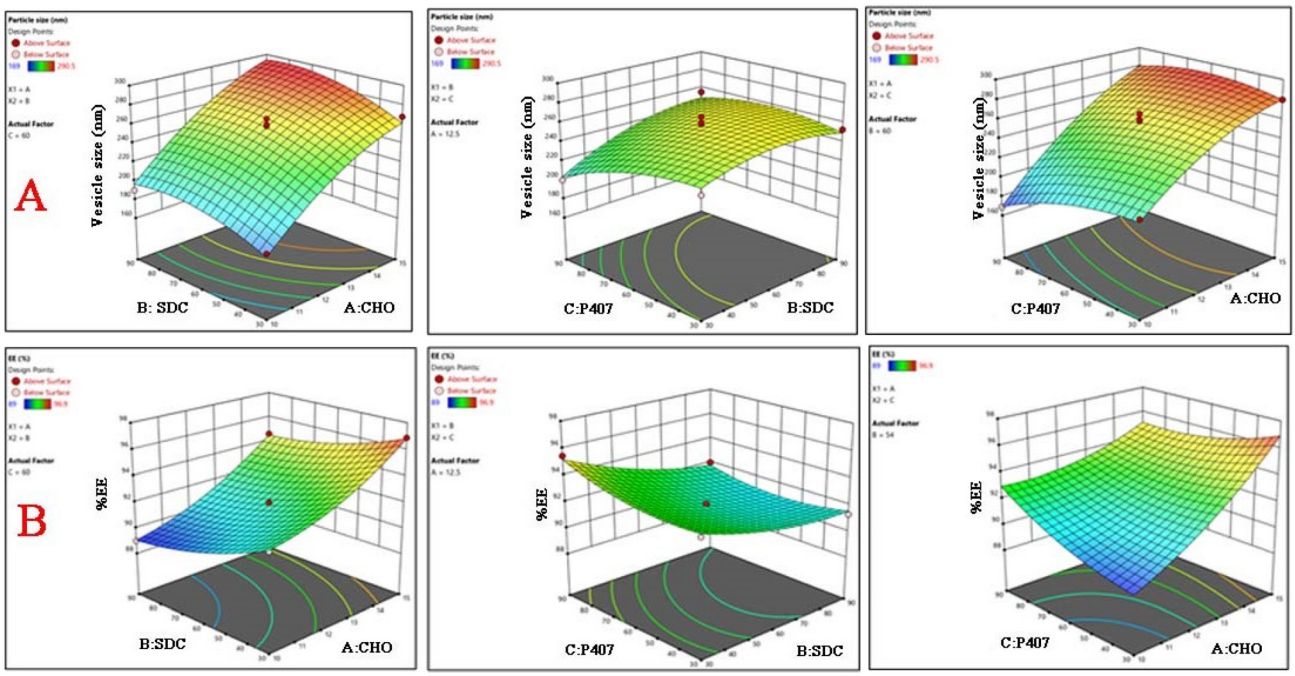

Fig. 1 Effects of simultaneous changes in independent variables on (A) vesicle size and (B) % entrapment efficiency.

deemed acceptable, the R^2 values that have been changed and projected must be within 0.2 of each other.[37]

3.1.2 Impact of independent variables on entrapment efficiency. The lowest and maximum percentage EE for all runs were found to be in the range 89%–96.9% w/w (Table 1). The impact of each independent variable on %EE can be seen in the 3D response surface plots in Fig. 1B. The polynomial equation (eqn (4)) obtained upon mathematical treatment of the data is:

$$\%EE = +91.80 + 2.55 \times A - 1.34 \times B + 0.4713 \times C + 0.1725 \times AB - 1.43 \times AC - 0.3625 \times BC + 0.7675 \times A^2 + 0.5500 \times B^2 + 0.6625 \times C^2 \quad (4)$$

The adjusted R^2 of 0.9646 suggested excellent correlation between %EE and the components used to prepare ART-BIL, in agreement with the projected R^2 of 0.8888. The direct relationship between CHO and %EE was demonstrated by the polynomial equation and Fig. 1B, whereby %EE increased with an increase in CHO concentration.

The optimal ART-loaded bilosomes were selected using Design-Expert software's mathematical optimization technique to diminish vesicle size and obtain the maximum value of % EE. Accordingly, the software's point prediction algorithm yielded the optimal formulation. The predicted (as per software) batch with CHO (11.06 mg), P407 (89.99 mg) and SDC (30 mg) levels had a vesicle size of 174.13 ± 3.15 nm and %EE of 94.86 ± 1.12%. The experimental homogeneously dispersed optimized batch (ART-BILopt) with ART (25 mg), CHO (11.06 mg), surfactant (Poloxamer 407, 89.99 mg), and BS (SDC, 30 mg) showed a vesicle size of 186.7 nm ± 1.92 nm with a PDI of 0.2 and %EE of 95.36 ± 2.11%, with 0.864 composite desirability and an adequate precision value of 4.37. The values of composite desirability and adequate precision suggest the suitability of the model to provide a strong and reliable prediction of the response. Furthermore, the prediction errors for VS and %EE were determined to be −6.73% and −0.52%, respectively, confirming the validity of the obtained responses.

3.2 Evaluation of artesunate-excipient compatibility using FTIR

The compatibility of ART with various bilosomes excipients was investigated using FTIR spectroscopy. The recorded spectra for ART, SDC, CDCA, CHO, P407, and ART-BILopt are shown in Fig. 2.

Prominent %transmittance bands at 3507 cm^{-1}, 1340 cm^{-1}, and 1750 cm^{-1} were seen in the FTIR spectra of ART. These bands were linked to the stretching of a tertiary amine group by the –OH group and $–NH_2$. The FTIR spectra of P407 and SDC revealed distinct bands at 1144 cm^{-1} and 1588 cm^{-1}, respectively, corresponding to C═O (carbonyl) stretch and C–O (ester). The distinctive stretching vibration bands for the –OH group at 3360 cm^{-1} and C–H stretching at 2935 cm^{-1} were observed in the FTIR spectra of CHO. The distinctive stretching vibration bands for the –COO group at 1706 cm^{-1} and CH_3 stretching at 2844 cm^{-1} were observed in the FTIR spectra of CDCA. ART-BILopt showed a shift in the %transmittance band of ART to 3560 cm^{-1}, corresponding to the –OH group, while the band for the C═O group present in CDCA showed a shift to 1715 cm^{-1}.

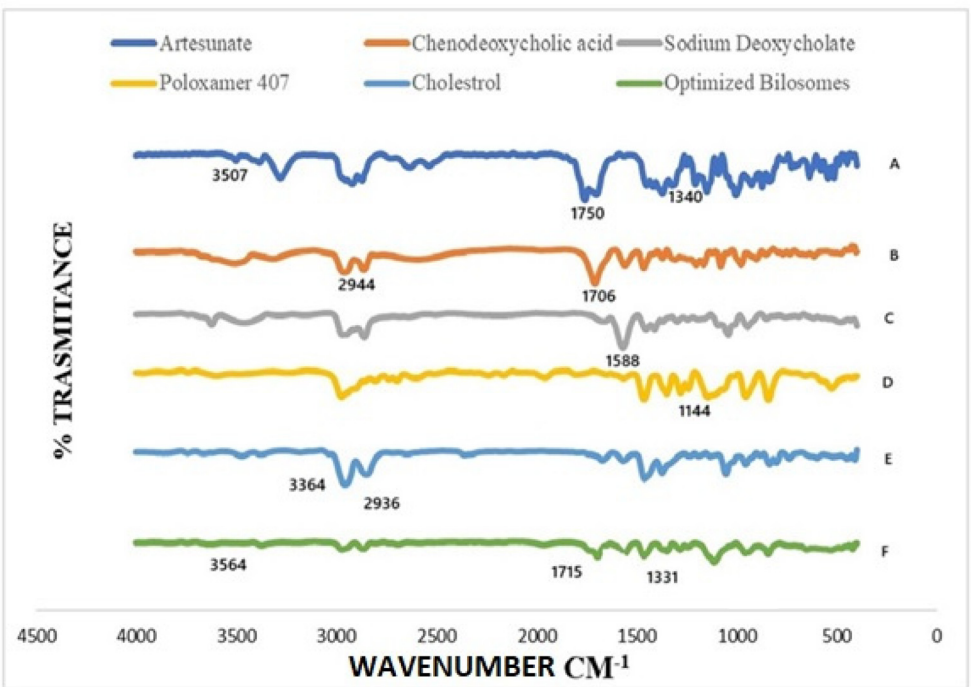

Fig. 2 FTIR spectra of (A) artesunate, (B) chenodeoxycholic acid, (C) sodium deoxycholate, (D) Poloxamer 407, (E) cholesterol and (F) ART-BILopt.

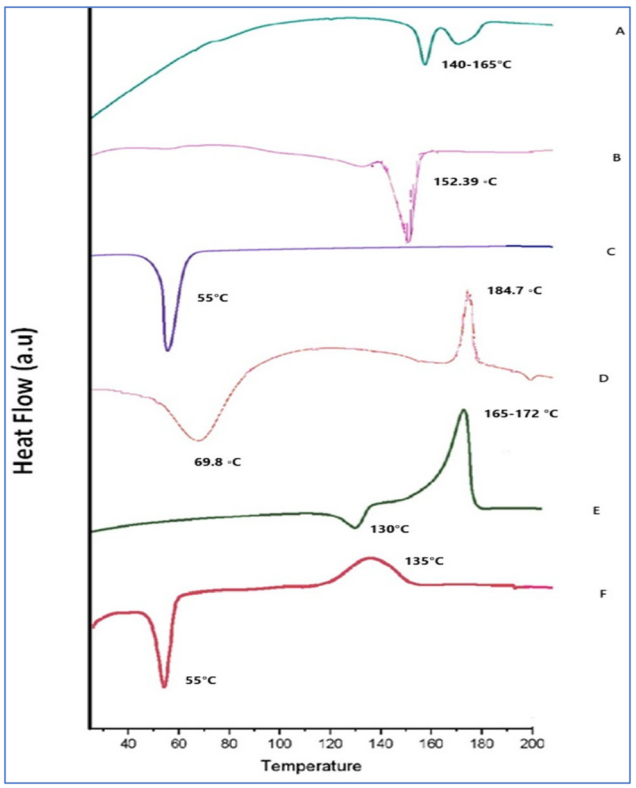

Fig. 3 DSC thermograms of (A) CDCA, (B) cholesterol, (C) Poloxamer 407, (D) sodium deoxycholate, (E) ART and (F) ART-BIL.

3.3 Thermal analysis of ART and excipient using DSC

The formulation and excipients were thermally analyzed using DSC (Fig. 3). The DSC thermograms of CHO and SDC displayed characteristic melting endothermic peak at 152.39 °C, and 69.8 °C respectively. Furthermore, at 184.7 °C, SDC showed an exothermic peak, which is believed to be associated with the recrystallization of its lipophilic chains. The DSC thermogram of P407 displayed a characteristic endothermic peak at a temperature of around 55 °C, representing its melting point. The melting point of CDCA was found roughly at 140 to 166 °C. This peak shows that when the material absorbs heat, it changes from a solid to a liquid state. ART is a crystalline material, which showed a characteristic endothermic peak at 130 °C corresponding to its melting point, and an exothermic peak between 165–172 °C.[38] ART-BIL showed an endothermic peak corresponding to the melting of P407 and an exothermic peak at 135 °C. Surprisingly, ART-BIL did not exhibit a peak of ART.

3.4 Examination of bilosome morphology using TEM

The shape, morphology, and average vesicle size of ART-BILopt were examined using TEM and particle size analyzer respectively (Fig. 4). Further vesicle size distribution histogram for the bilosomes under analysis is presented in Fig. 4A. The photomicrograph show vesicles with a spherical shape and no clumps (Fig. 4B).

3.5 *In vitro* drug release study of ART-BIL

A dynamic dialysis method was used to measure the *in vitro* release of ART. To estimate the possibility of vesicular disruption under physiological settings, release studies for ART-BIL and the ART dispersion were carried first at pH 1.2 and then at pH 6.8. The ART-BIL release profile was found to be biphasic in nature with an initial burst release of ART (about 20%) followed by around 89% of ART release in a 24 h period (Fig. 5). Furthermore, the *in vitro* release of ART from the aqueous dispersion showed a cumulative drug release of 31% over a 24 h period.

3.6 Estimation of binding potential of ART and CDCA using an *in silico* docking study

In silico molecular docking studies were performed to investigate the binding potential of ART and CDCA (ligands) to glyceraldehyde 3-phosphate dehydrogenase (G3PDH) identified

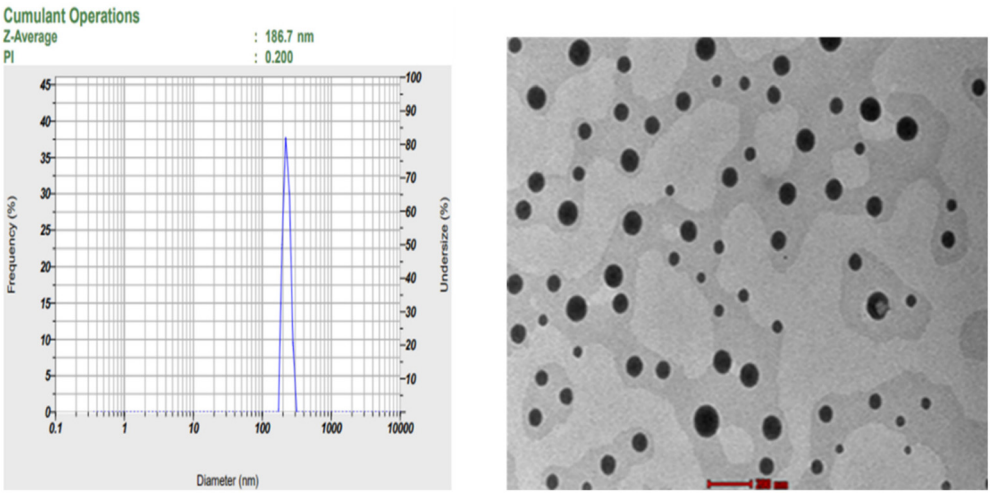

Fig. 4 (A) Vesicle size distribution of ART-BILopt. (B) TEM of ART-BILopt.

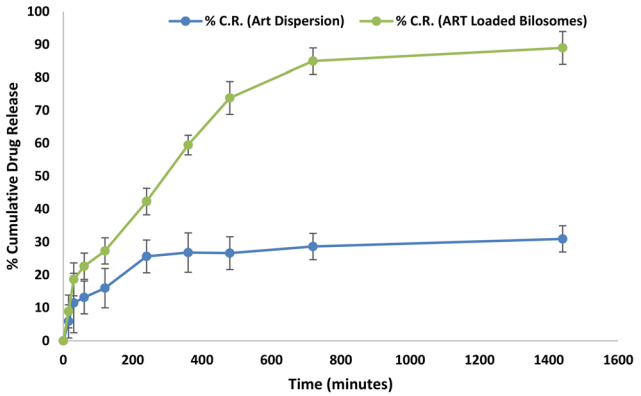

Fig. 5 *In vitro* release profile of the ART from the ART dispersion and ART-BILopt.

as the target receptor. It is commonly established that the binding energies and affinities of both ligands with the protein under study are directly correlated. ART exhibited the highest affinity for G3PDH (Fig. 6), suggesting its potential as an antileishmanial agent. Similar studies were conducted with CDCA as the ligand (Table 2), which also showed a strong affinity for the selected receptor, suggesting that it also possesses antileishmanial potential. CDCA demonstrated the highest binding energy for the G3PDH enzyme. Furthermore, we performed a study of *in vitro* antileishmanial activity to confirm the observations of the *in silico* docking studies.

3.7 *In vitro* evaluation of ART-BIL against leishmanial promastigotes

It was observed that ART-BILopt (A-Bs) are ~5-fold more effective at killing the parasite after 48 h of treatment than

Table 2 Binding energy of ART and CDCA against enzyme glyceraldehyde 3-phosphate dehydrogenase involved in glycolytic pathway of leishmanial parasite

Ligand	Protein	Binding energy (kcal mol^{-1})	Amino acid residues
Artesunate	Glyceraldehyde 3-phosphate dehydrogenase	−8.2	ASN-275 GLU-300 ARG-274
CDCA	Glyceraldehyde 3-phosphate dehydrogenase	−8.7	SER-155 LYS-125 GLY-24

ART alone (Fig. 7). This is because the IC_{50} of A-Bs is 10 μg mL^{-1}, whereas for ART it is 50 μg mL^{-1} after 48 h ($P < 0.001$, Fig. 7A). AmB, used as a positive control, kills the parasite in a time-dependent manner, as expected. We observed ~50% and 28% survival of promastigotes after AmB (50 nM) treatment for 48 and 72 h, respectively. The parasite survival was ~83% and ~80% after 48 h when the cells were treated with 50 μg mL^{-1} of blank bilosomes (B) and bile salt (Bs), respectively (Fig. 7A). The parasite survival after 72 h was ~82% and 84% for blank bilosomes and bile salt treatment, respectively (Fig. 7B). However, after 72 h, the parasite survival was only 29% and 3% for 50 μg mL^{-1} of ART and A-Bs treated parasites, respectively ($P < 0.001$, Fig. 7B).

3.8 *In vivo* pharmacokinetic evaluation of ART-BIL

The pharmacokinetic characteristics of ART-BILopt and ART dispersion after oral administration are displayed in Fig. 8. The results of various pharmacokinetic parameters are shown in Table 3. Animals treated with customized bilosomes exhibited significantly higher plasma concentrations of ART during

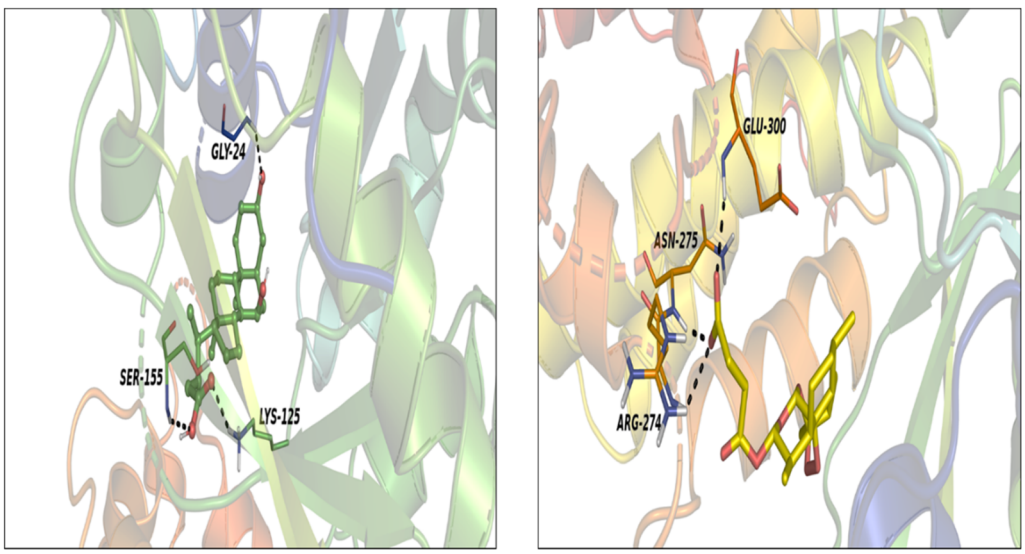

Fig. 6 Docking results of (A) the interaction of artesunate with amino acid chemical residues (GLU-300), (ASN-275), (ARG-274), and (B) the interaction of chenodeoxycholic acid with amino acid chemical residues (GLY-24), (SER-155), (LYS-125) by forming H-bonds with glyceraldehyde 3-phosphate dehydrogenase (PDB ID 1M67).

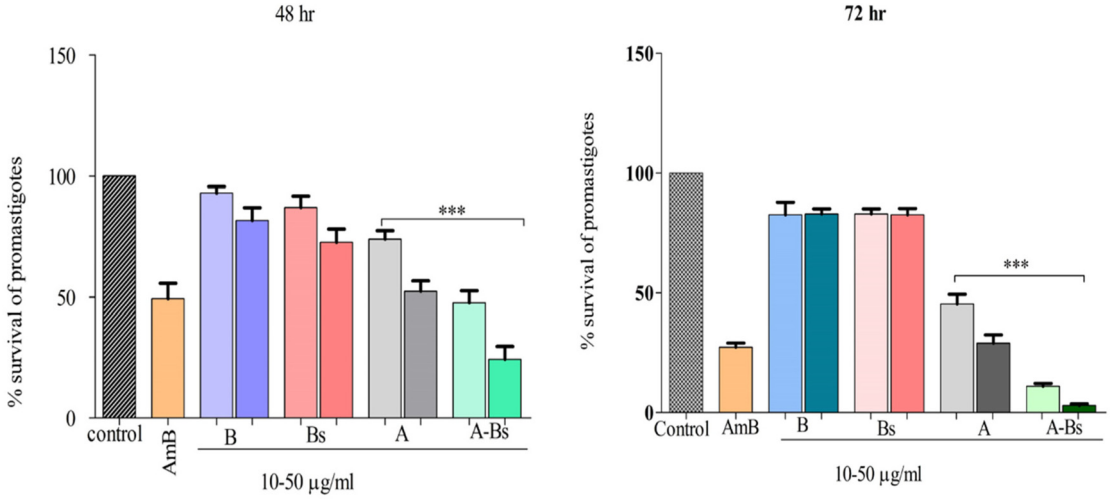

Fig. 7 Antileishmanial activity of ART (A), blank bilosomes (B), bile salt (Bs), ART-BIL (A-Bs), amphotericin B (AmB), against *Leishmania donovani* promastigote.

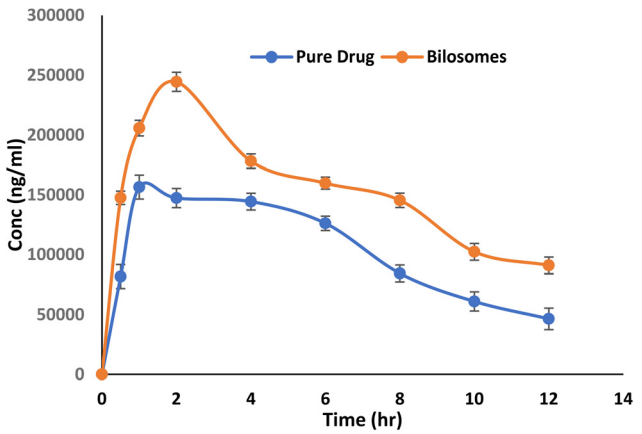

Fig. 8 Plasma concentration–time profiles of ART in rats following oral ART suspension and ART-BILopt administration.

Table 3 Pharmacokinetic parameters of artesunate after oral administration of ART-BIL and ART dispersion

Parameter	ART dispersion	ART-BIL
C_{max} (ng mL^{-1})	165 034.1 ± 150	229 878.4 ± 336*
AUC_{0-t} (ng mL^{-1} h^{-1})	1 272 179 ± 212	1 875 934 ± 510*
$AUC_{0-\infty}$ (ng mL^{-1} h^{-1})	1 652 383 ± 415	2 770 366 ± 735*
$t_{1/2}$ (h)	5.216407 ± 0.28	6.97205 ± 0.30
T_{max} (h)	2	1.12

Mean ± SD, *Statistically significant compared with ART dispersion ($P < 0.05$).

all time periods compared to animals given the ART dispersion. ART-BILopt had a C_{max} value of 229 878.4047 ± 336 ng mL^{-1}, which was 1.39 times higher ($P < 0.05$) than that of the ART dispersion (165 034.129 ± 150 ng mL^{-1}). Likewise, AUC_{0-24} and $AUC_{0-\infty}$ of ART-BILopt were found to be (1 875 934.095 ± 510 ng h mL^{-1}) and (2 770 366 ± 735 ng h mL^{-1}), which differ significantly ($P < 0.05$) from the AUC_{0-24} and $AUC_{0-\infty}$ of the ART dispersion (1 272 179.324 ± 212 ng h mL^{-1}) and (1 652 383 ± 435 ng h mL^{-1}), suggesting 1.47 and 0.59 fold increases, respectively, compared to the ART dispersion. The half-lives of ART-BIL and the ART dispersion are 6.97205 ± 0.30 h and 5.216407 ± 0.28 h, respectively. The T_{max} of ART-BIL is roughly 0.85 times greater than that of the ART dispersion, indicating that ART achieves its maximum concentration marginally sooner when formulated into BIL.

4. Discussion

The optimization ART-BIL was undertaken using BBD, which is well known for investigating the impacts of independent variables on a dependent one. Further, as stated earlier, the positive CHO coefficient showed a direct relationship between the quantity of CHO and the vesicle size, signifying that when the CHO concentration increases, so does the vesicle size of ART-BIL. This behaviour could be attributed to the system's elevated mass. CHO has lipid chains that are flexible and might have aided the capture of more aqueous solution inside BIL, displaying an increase in the size of the vesicles. Furthermore, an increase in CHO greatly increased the amount of ART entrapment in the vesicles, leading to their enlargement. Surfactants had the opposite influence on vesicle size. They might have reduced the interfacial tension between the water and cholesterol, which in turn reduced their distance from one another and resulted in a subsequent reduction in vesicle size. Moreover, the histogram of particle size distribution and vesicle size demonstrated by TEM data agreed quite well.

Similarly, the impact of independent variables on %EE was investigated. The hydrophobicity and stiffness of the lipid bilayer increased with CHO, which could have resulted in

increased ART encapsulation and stability in the bilosome vesicles.[39] Additionally, SDC (B) and P407 (C) concentration also showed a positive effect on the %EE of ART in BIL. Increases in the amounts of SDC and P407 resulted in decreased interfacial tension with a subsequent rise in viscosity, which stopped ART from escaping from BIL. However, at higher amounts of SDC, a reduction in %EE was observed. The fluidizing effect produced by bile salts on the lipid bilayers, which ends up in ART leakage, could be responsible for a decrease in %EE. The shifts in the %transmittance bands of ART and CDCA, as depicted by FTIR studies, suggested the likelihood of hydrogen bonding between them. This could have been the reason for entrapment of ART within the bilosomes. DSC studies confirmed the molecular distribution of ART within the bilosomes, as the prepared ART-BIL did not display the characteristic endotherm for ART. Yet another reason for such behaviour could be associated with the solubilisation of ART in molten CHO and P407.[40]

The *in vitro* drug release study demonstrated the initial burst release of ART from ART-BIL, which could be attributed to the release of ART molecules adsorbed on the surface of BIL. The extended release of ART from the bilosomes was caused by the significant affinity of ART for the hydrophobic counterpart of the vesicles. The results of the *in vitro* drug release study suggested a significant enhancement (2.8 fold) in the dissolution rate of ART when formulated into bilosomes. This could be attributed to the nanosize of BIL, which might have provided an enormous surface area for the dissolution of ART.

It was hypothesized that the inclusion of CDCA into bilosomes would enhance the antileishmanial effect of ART as a synergistic activity. *In silico* molecular docking studies confirmed our hypothesis about using CDCA as one of the formulation components, as it suggested the likelihood of synergistic antileishmanial activity when combined with ART. Further *in vitro* antileishmanial activity studies indicated that the bilosomes themselves are not antileishmanial compared to ART alone, but ART-BIL, as a formulation, is a more effective antileishmanial agent than ART alone. Bile-salt-based drug delivery against leishmania was earlier proven to be effective for drugs, where poor solubility and chemical instability were improved due to the bile-salt-based formulation. Further, the prepared ART-BIL when tested *in vivo* in rats showed significant enhancement in C_{max} and AUC_{0-24} of ART when formulated into BIL. This could be attributed to reduced vesicle size (nanosize), increased ART entrapment in the bilosome vesicles, and avoidance of first-pass metabolism as the BIL gets absorbed through Peyer's patches.

5. Conclusion

In the current investigation, artesunate-loaded bilosomes were prepared and optimized using Box–Behnken design. The optimized formulation had a vesicle size of 186.7 ± 2.7 nm and an entrapment efficiency of 95.36 ± 2.11%. Spherical, non-aggregated vesicles demonstrated a biphasic drug release profile with a remarkable increase in dissolution rate of artesunate compared to an artesunate dispersion. *In silico* molecular docking studies revealed the antileishmanial potential of artesunate and chenodeoxycholic acid by binding to glyceraldehyde 3-phosphate dehydrogenase (G3PDH) and thus in turn the suppression of glycolysis. Further, *in vitro* antileishmanial studies showed significant enhancement in the antileishmanial potential of artesunate.

Abbreviations

ART	Artesunate
BIL	Bilosomes
ART-BIL	ART-loaded bilosomes
CDCA	Chenodeoxycholic acid
BBD	Box–Behnken design
VL	Visceral leishmaniasis
FTIR	Fourier transform-infrared spectroscopy
PXRD	Powder X-ray diffraction
SEM	Scanning electronic microscopy
DSC	Differential scanning calorimetry

Ethics approval and consent to participate

Animal experimentation procedures were followed in accordance with CPCSEA guidelines.

Data availability

The datasets generated during and/or analysed during the current study are available from the corresponding author on reasonable request.

Conflicts of interest

The authors report no conflict of interest to declare.

References

1 D. Steverding, The history of leishmaniasis, *Parasites Vectors*, 2017, **10**, 82, DOI: **10.1186/s13071-017-2028-5**.
2 J. Seaman, Epidemic Visceral Leishmaniasis in Southern Sudan: Treatment of Severely Debilitated Patients under Wartime Conditions and with Limited Resources, *Ann. Intern. Med.*, 1996, **124**, 664, DOI: **10.7326/0003-4819-124-7-199604010-00007**.
3 J. van Griensven and E. Diro, Visceral Leishmaniasis, *Infect. Dis. Clin. North Am.*, 2012, **26**, 309–322, DOI: **10.1016/j.idc.2012.03.005**.

4 B. Ayi, *Leishmaniasis. xPharm Compr. Pharmacol. Ref*, Elsevier, 2007, pp. 1–10. DOI: 10.1016/B978-008055232-3.60933-X.
5 K. P. Chang and D. Fong, Cell biology of host-parasite membrane interactions in leishmaniasis, *Ciba Found. Symp.*, 1983, **99**, 113–137, DOI: 10.1002/9780470720806.ch7.
6 S. Jain, U. Sahu, A. Kumar and P. Khare, Metabolic Pathways of Leishmania Parasite: Source of Pertinent Drug Targets and Potent Drug Candidates, *Pharmaceutics*, 2022, **14**, 1590, DOI: 10.3390/pharmaceutics14081590.
7 A. Mirzaei, M. Maleki, E. Masoumi and N. Maspi, A historical review of the role of cytokines involved in leishmaniasis, *Cytokine*, 2021, **145**, 155297, DOI: 10.1016/j.cyto.2020.155297.
8 M. Ohms, C. Ferreira, H. Busch, I. Wohlers, A. C. Guerra de Souza, R. Silvestre, *et al.* Enhanced Glycolysis Is Required for Antileishmanial Functions of Neutrophils Upon Infection With Leishmania donovani, *Front. Immunol.*, 2021, **12**, 1–14, DOI: 10.3389/fimmu.2021.632512.
9 R. J. S. Burchmore and M. P. Barrett, Life in vacuoles – nutrient acquisition by Leishmania amastigotes, *Int. J. Parasitol.*, 2001, **31**, 1311–1320, DOI: 10.1016/S0020-7519(01)00259-4.
10 A. T. Cordeiro, R. Hardré, P. A. M. Michels, L. Salmon, L. F. Delboni and O. H. Thiemann, Leishmania mexicana mexicana glucose-6-phosphate isomerase: Crystallization, molecular-replacement solution and inhibition, *Acta Crystallogr., Sect. D:Biol. Crystallogr.*, 2004, **60**, 915–919, DOI: 10.1107/S0907444904003762.
11 K. Nyame, D.-T. Chuong Dai, R. Opperdoes Fred and P. A. M. Michels, Subcellular distribution and characterization of glucosephosphate isomerase in Leishmania mexicana mexicana, *Mol. Biochem. Parasitol.*, 1994, **67**, 269–279, DOI: 10.1016/0166-6851(94)00139-1.
12 C. L. M. J. Verlinde, V. Hannaert, C. Blonski, M. Willson, J. J. Périé, L. A. Fothergill-Gilmore, *et al.* Glycolysis as a target for the design of new anti-trypanosome drugs, *Drug Resistance Updates*, 2001, **4**, 50–65, DOI: 10.1054/drup.2000.0177.
13 D. J. Rigden, S. E. Phillips, P. A. Michels and L. A. Fothergill-Gilmore, The structure of pyruvate kinase from Leishmania mexicana reveals details of the allosteric transition and unusual effector specificity, *J. Mol. Biol.*, 1999, **291**, 615–635, DOI: 10.1006/jmbi.1999.2918.
14 I. Kursula and R. K. Wierenga, Crystal structure of triosephosphate isomerase complexed with 2-phosphoglycolate at 0.83 Å resolution, *J. Biol. Chem.*, 2003, **278**, 9544–9551, DOI: 10.1074/jbc.M211389200.
15 Ş. Özsoylu, Treatment of visceral leishmaniasis, *Turk. J. Pediatr.*, 2003, **45**, 280, DOI: 10.4103/0974-777x.62883.
16 Z. Ma, W. Chen, Y. Liu, L. Yu, X. Mao, X. Guo, *et al.* Artesunate Sensitizes human hepatocellular carcinoma to sorafenib via exacerbating AFAP1L2-SRC-FUNDC1 axis-dependent mitophagy, *Autophagy*, 2024, **20**, 541–556, DOI: 10.1080/15548627.2023.2261758.
17 Z. j. Li, H. q. Dai, X. w. Huang, J. Feng, J. h. Deng, Z. x. Wang, *et al.* Artesunate synergizes with sorafenib to induce ferroptosis in hepatocellular carcinoma, *Acta Pharmacol. Sin.*, 2021, **42**, 301–310, DOI: 10.1038/s41401-020-0478-3.
18 Z. Huang, S. Gan, X. Zhuang, Y. Chen, L. Lu, Y. Wang, *et al.* Artesunate Inhibits the Cell Growth in Colorectal Cancer by Promoting ROS-Dependent Cell Senescence and Autophagy, *Cells*, 2022, **11**, 2472, DOI: 10.3390/cells11162472.
19 A. L. Greenshields, W. Fernando and D. W. Hoskin, The anti-malarial drug artesunate causes cell cycle arrest and apoptosis of triple-negative MDA-MB-468 and HER2-enriched SK-BR-3 breast cancer cells, *Exp. Mol. Pathol.*, 2019, **107**, 10–22, DOI: 10.1016/j.yexmp.2019.01.006.
20 M. J. Mutiso, C. J. Macharia, M. Barasa, E. Taracha, A. J. Bourdichon and M. M. Gicheru, Estudo in vitro e in vivo da eficácia anti leishmaniótica de terapêutica combinada de Diminazene e Artesunate contra Leishmania donovani em camundongos Balb/c, *Rev. Inst. Med. Trop. Sao Paulo*, 2011, **53**, 129–132, DOI: 10.1590/S0036-46652011000300003.
21 G. Geroldinger, M. Tonner, J. Quirgst, M. Walter, S. De Sarkar, L. Machín, *et al.* Activation of artemisinin and heme degradation in Leishmania tarentolae promastigotes: A possible link, *Biochem. Pharmacol.*, 2020, **173**, 113737, DOI: 10.1016/j.bcp.2019.113737.
22 P. Ji, H. Huang, S. Yuan, L. Wang, S. Wang, Y. Chen, *et al.* ROS-Mediated Apoptosis and Anticancer Effect Achieved by Artesunate and Auxiliary Fe(II) Released from Ferriferous Oxide-Containing Recombinant Apoferritin, *Adv. Healthc. Mater.*, 2019, **8**, 1900911, DOI: 10.1002/adhm.201900911.
23 B. J. Boyd, C. A. S. Bergström, Z. Vinarov, M. Kuentz, J. Brouwers, P. Augustijns, *et al.* Successful oral delivery of poorly water-soluble drugs both depends on the intraluminal behavior of drugs and of appropriate advanced drug delivery systems, *Eur. J. Pharm. Sci.*, 2019, **137**, 104967, DOI: 10.1016/j.ejps.2019.104967.
24 H. Kaurav, M. Tripathi, S. D. Kaur, A. Bansal, D. N. Kapoor and S. Sheth, Emerging Trends in Bilosomes as Therapeutic Drug Delivery Systems, *Pharmaceutics*, 2024, **16**, 697, DOI: 10.3390/pharmaceutics16060697.
25 R. Abdel-moneum and R. S. Abdel-Rashid, Bile salt stabilized nanovesicles as a promising drug delivery technology: A general overview and future perspectives, *J. Drug Delivery Sci. Technol.*, 2023, **79**, 104057, DOI: 10.1016/j.jddst.2022.104057.
26 E. Zarenezhad, M. Marzi, H. T. Abdulabbas, S. A. Jasim, S. A. Kouhpayeh, S. Barbaresi, *et al.* Bilosomes as Nanocarriers for the Drug and Vaccine Delivery against Gastrointestinal Infections: Opportunities and Challenges, *J. Funct. Biomater.*, 2023, **14**, 453, DOI: 10.3390/jfb14090453.

27 E. Moghimipour, A. Ameri and S. Handali, Absorption-Enhancing Effects of Bile Salts, *Molecules*, 2015, **20**, 14451–14473, DOI: **10.3390/molecules200814451**.

28 W. L. Masiiwa and L. L. Gadaga, Intestinal Permeability of Artesunate-Loaded Solid Lipid Nanoparticles Using the Everted Gut Method, *Drug Delivery*, 2018, **2018**, 1–9, DOI: **10.1155/2018/3021738**.

29 V. R. Gogulamudi, M. L. Dubey, D. Kaul, D. J. Hubert, R. Kandimalla and R. Sehgal, Vitamins (A&D) and Isoprenoid (Chenodeoxycholic acid) molecules are accompanied by Th1 immunostimulatory response and therapeutic cure in vivo: possible antileishmanial drugs, *Sci. Rep.*, 2019, **9**, 8531, DOI: **10.1038/s41598-019-44630-4**.

30 S. Patil, S. Bahadure and S. Patil, Formulation of canagliflozin hemihydrate-loaded bilosomes for the treatment of Type-2 diabetes mellitus: In vitro, in vivo and in silico molecular docking studies, *J. Drug Delivery Sci. Technol.*, 2023, **86**, 104630, DOI: **10.1016/j.jddst.2023.104630**.

31 S. Patil, V. Ujalambkar, A. Rathore, S. Rojatkar and V. Pokharkar, Galangin loaded galactosylated pluronic F68 polymeric micelles for liver targeting, *Biomed. Pharmacother.*, 2019, **112**, 108691, DOI: **10.1016/j.biopha.2019.108691**.

32 P. Kumar, P. Shivam, S. Mandal, P. Prasanna, S. Kumar, S. R. Prasad, *et al.* Synthesis, characterization, and mechanistic studies of a gold nanoparticle-amphotericin B covalent conjugate with enhanced antileishmanial efficacy and reduced cytotoxicity, *Int. J. Nanomed.*, 2019, **14**, 6073–6101, DOI: **10.2147/IJN.S196421**.

33 S. R. Prasad, P. Kumar, S. Mandal, A. Mohan, R. Chaurasia, A. Shrivastava, *et al.* Mechanistic insight into the role of mevalonate kinase by a natural fatty acid-mediated killing of Leishmania donovani, *Sci. Rep.*, 2022, **12**, 16453, DOI: **10.1038/s41598-022-20509-9**.

34 E. Kupetz, L. Preu, C. Kunick and H. Bunjes, Parenteral formulation of an antileishmanial drug candidate - Tackling poor solubility, chemical instability, and polymorphism, *Eur. J. Pharm. Biopharm.*, 2013, **85**, 511–520, DOI: **10.1016/j.ejpb.2013.02.001**.

35 P. L. Olliaro, N. K. Nair, K. Sathasivam, S. M. Mansor and V. Navaratnam, Pharmacokinetics of artesunate after single oral administration to rats, *BMC Pharmacol.*, 2001, **1**, 12, DOI: **10.1186/1471-2210-1-12**.

36 F. H. A. Nogueira, N. F. A. Reis, P. R. Chellini, I. da C. César and G. A. Pianetti, Development and validation of an HPLC method for the simultaneous determination of artesunate and mefloquine hydrochloride in fixed-dose combination tablets, *Braz. J. Pharm. Sci.*, 2013, **49**, 837–843, DOI: **10.1590/S1984-82502013000400024**.

37 A. Gouda, O. S. Sakr, M. Nasr and O. Sammour, Ethanol injection technique for liposomes formulation: An insight into development, influencing factors, challenges and applications, *J. Drug Delivery Sci. Technol.*, 2021, **61**, 102174, DOI: **10.1016/j.jddst.2020.102174**.

38 R. Chadha, S. Gupta, G. Shukla, D. V. S. Jain, R. R. S. Pissurlenkar and E. C. Coutinho, Interaction of artesunate with β-cyclodextrin: Characterization, thermodynamic parameters, molecular modeling, effect of PEG on complexation and antimalarial activity, *Results Pharma Sci.*, 2011, **1**, 38–48, DOI: **10.1016/j.rinphs.2011.07.002**.

39 A. Can, A. I. I. Tyler and A. R. Mackie, Potential use of bile salts in lipid self-assembled systems for the delivery of phytochemicals, *Curr. Opin. Colloid Interface Sci.*, 2021, **56**, 101502, DOI: **10.1016/j.cocis.2021.101502**.

40 S. S. Patil, K. Roy, B. Choudhary and K. R. Mahadik, Fabrication of novel GMO/Eudragit E100 nanostructures for enhancing oral bioavailability of carvedilol, *Drug Dev. Ind. Pharm.*, 2016, **42**, 1300–1307, DOI: **10.3109/03639045.2015.1128440**.